Indonesian Journal of Electronics, Electromedical Engineering, and Medical Informatics e-ISSN: 2656-8624
Homepage: https://ijeeemi.org/; Vol. 7, No. 2, pp. 331-343, May 2025

RESEARCH PAPER

OPEN ACCES

Multi-Channel Trans-Admittance Imaging for Anomaly Detection

Fransiska Maria Aprihapsari[1], Atin Asna Octavia[1], Khushnul Ain[2], and Bayu Ariwanto[3]

[1] Master of Biomedical Engineering, Universitas Airlangga, Surabaya, Indonesia
[2] Biomedical Engineering Innovation Research Group, Faculty of Science and Technology, Universitas Airlangga, Surabaya, Indonesia
[3] Department of Physic, Universitas Airlangga, Surabaya, Indonesia

ABSTRACT

This research aims to develop an Electrical Impedance Tomography (EIT) system to detect anomalies in the network. The developed system utilizes 64 copper-based electrodes and Analog Discovery 2 as a real-time sinusoidal current source. The frequencies used are 50, 80, 100, 120, and 150 kHz because these frequency ranges are able to capture differences in network conductivity values. Each time data is captured, the system generates three main values, namely real, imaginary, and magnitude impedance values, each of which represents the conductivity conditions in the measurement area at 64 electrode points. The values are then converted into RGB format and mapped to be visualized in the form of an 8-bit digital image. In the reconstructed image, areas with significant differences in conductivity will appear with increasingly brownish shades of color, indicating a potential anomaly. The anomaly detection method in this study uses a 0.9% NaCl saline solution as the main medium. As a model of tissue anomalies, natural materials such as jicama and carrots are used. The anomaly position is varied at distances of 4 cm, 5 cm, 6 cm, and 7 cm, which is adjusted to the dimensions of the available acrylic containers to ensure systematic evaluation of the system against detection sensitivity at various depths. The results showed that the system was able to detect the difference in conductivity values between the anomaly and the anomalous area. Higher conductivity values are consistently measured in areas where anomalies are present compared to areas where there are no anomalies. The most optimal detection occurs at a measurement distance of 4 cm, as well as at the lowest frequency, which is 50 kHz.This method is an innovative solution for non-invasive and safe detection of tissue anomalies, without exposure to ionizing radiation, making it suitable for early diagnostic procedures in various medical fields, such as breast cancer detection, tumor identification, and other diagnostic applications. In addition, the system is low-cost and easy to use because the result is a visual image that makes it easy for medical personnel to interpret and analyze.

PAPER HISTORY

Received Feb. 10, 2025
Accepted April 30, 2025
Published May 3, 2025

KEYWORDS

Impedance tomography;
Spectroscopy;
Trans-admittance imaging;
Multichannel electrodes;
Anomaly detection

AUTHOR EMAIL

fransiska.maria.aprihapsari-2023@fst.unair.ac.id
atin.asna.octavia-2024@fst.unair.ac.id
k_ain@fst.unair.ac.id
bayuariwanto@staf.unair.ac.id

1. INTRODUCTION

Electrical Impedance Tomography (EIT) is a non-invasive imaging technology that maps the impedance distribution of body tissues by injecting electrical currents and measuring the resulting voltage [1], [2]. The impedance of body tissues consists of two components: real resistance and imaginary capacitive reactance, which are essential for medical applications [2]. EIT detects abnormalities in body tissues based on impedance differences between normal and abnormal tissues [3], [4]. This technology is often applied in medical cases, including breast cancer detection, where experiments have shown that breast cancer tissues have lower impedance than normal tissues, making impedance-based imaging a promising tool for diagnosis [3].

Multi-frequency Electrical Impedance Tomography (Mf-EIT) [2], [5], [6] is a type of EIT which produces many structural images for different frequencies. The resulting image is an impedance distribution as a function of frequency. This technique involves injecting alternating electrical currents at multiple frequencies through electrodes and measuring the resulting voltages. The frequency-dependent conductivity data helps distinguish different types of tissues or anomalies [7], [8]. The anomalies detected are carrot and jicama, which were selected based on a similar approach, where carrots were used as anomalous materials [2]. The selection of carrots

Corresponding author: Khushnul Ain, k_ain@fst.unair.ac.id, Biomedical Engineering Innovation Research Group, Faculty of Science and Technology, Universitas Airlangga, Surabaya, Indonesia
Digital Object Identifier (**DOI**): https://doi.org/10.35882/ijeeemi.v7i2.88
Copyright © 2025 by the authors. Published by Jurusan Teknik Elektromedik, Politeknik Kesehatan Kemenkes Surabaya Indonesia. This work is an open-access article and licensed under a Creative Commons Attribution-ShareAlike 4.0 International License (CC BY-SA 4.0).

was based on their distinct impedance properties compared to the surrounding medium, enabling clear identification of anomalies in the imaging process. Jicama (Pachyrhizus erosus) was chosen as the main background material due to its high water content and relatively uniform impedance, mimicking biological soft tissues. Carrots, with denser structure and lower water content, provide sufficient contrast in impedance when placed inside jicama, thus simulating the presence of an anomaly in tissue imaging. Previous studies have successfully employed carrots as test anomalies due to their reproducible and distinguishable electrical characteristics [2], [7]. In EIT, a saline solution like NaCl 0,9% can be used as the conductive medium. The conductivity of NaCl solution provides a stable background for detecting anomalies [7], [9], [10]

Analog Discovery 2 is a versatile, multifunctional tool that can simultaneously control and generate currents at various frequencies. It can function as a digital oscilloscope that can record and visualize measurement data, making it an ideal instrument for handling mixed-signal circuits in one compact device [11]

In this study, we address the need for non-invasive and cost-effective imaging techniques capable of detecting anomalies within biological tissues [12], [13] Previous studies have demonstrated the feasibility of using EIT for anomaly detection [6], [14]. In addition, Wi H. et al. developed a multi-frequency EIT system with automatic self-calibration using 16 electrodes [15]. Tan et al. introduced a wideband EIT system that utilized 16 and 32 electrodes [16]. Sapuan et al. developed an EIT using 16 electrodes, where alternating currents are injected using frequencies of 10-100 kHz to produce three types of images: impedance, real impedance, and imaginary impedance [2]. Furthermore, the collected voltage data is used to reconstruct images of the conductivity distribution [10], [12], [13]. In this study, the selected frequencies of 50, 80, 100, 120, and 150 kHz were chosen based on prior studies indicating that biological tissues show significant impedance variation within this range, allowing better discrimination of anomalies. These frequencies also fall within the operational bandwidth of Analog Discovery 2, ensuring stable and accurate data acquisition. Through the Linear Back Projection (LBP) reconstruction method and the separation of impedance components based on the phase difference between potential and current, they showed that real and imaginary functional images are more sensitive in detecting anomalies compared to overall impedance images, especially when the anomalies are represented by materials such as carrots [2]. Carrots were again employed as anomalous materials in the study "Detection of Multicomponent Distribution by Electrical Impedance Spectroscopic Tomography" by Wang Yao et al. These studies collectively underscore the potential of EIT for anomaly detection, while also highlighting the limitations of lower electrode counts that our research aims to overcome.

However, many of these systems employed a limited number of electrodes, which constrained spatial resolution and detection sensitivity. Additionally, traditional EIT systems often relied on separate current sources and switching mechanisms, which can lead to increased system complexity and reduced real-time imaging capabilities. To overcome these limitations, this study aims to develop an EIT with Analog Discovery 2 as an integrated real-time sinusoidal current source, combined with a multiplexer to deliver current to 64 electrode points. This approach aims to enhance spatial resolution and detection accuracy. Despite these advancements, challenges remain, including the need to manage increased data complexity and ensure the stability of measurements across a higher number of electrodes. The contributions of this study are 1) the use of 64 copper-based electrodes to improve spatial resolution 2) the implementation of Analog Discovery 2 as a sinusoidal current source, allowing the injection of sinusoidal current at a wide range of frequencies in real-time using a simpler circuit. 3) simple system and low cost because the developed system is easy to use. 4) the system generates 8-bit images by integrating real, imaginary, and magnitude impedance values, facilitating easier interpretation and analysis. Specifically, this research aims to:

1. Evaluate the feasibility of using multi-channel EIT for detecting tissue anomalies by leveraging simultaneous data acquisition from 64 electrodes to enhance spatial resolution and detection accuracy.
2. Improve anomaly detection by generating comprehensive impedance-based images that integrate real, imaginary, and magnitude values into an 8×8-bit RGB format, thereby facilitating easier interpretation.
3. Assess the performance and reliability of the Analog Discovery 2 as a real-time sinusoidal current source in multi-frequency impedance measurements at 50, 80, 100, 120, and 150 kHz.
4. Establish the foundation for a robust EIT system capable of capturing impedance differences across multiple regions simultaneously, offering valuable insights for tissue identification and anomaly detection analysis.

Thus, this research is expected to make a significant contribution to the development of advanced, non-invasive, and cost-effective imaging techniques for early detection of tissue anomalies, paving the way for improved diagnostic applications in medical settings. This study is structured as follows: Section II details the design of both hardware and software, the preparation of anomaly models, and the data acquisition process. Section III presents the experimental results and analysis. Section IV offers a discussion and comparison of the findings with previous studies, including an evaluation of the system's limitations. Section V provides the conclusions and potential improvements.

Corresponding author: Khushnul Ain, k_ain@fst.unair.ac.id, Biomedical Engineering Innovation Research Group, Faculty of Science and Technology, Universitas Airlangga, Surabaya, Indonesia
Digital Object Identifier (**DOI**): https://doi.org/10.35882/ijeeemi.v7i2.88
Copyright © 2025 by the authors. Published by Jurusan Teknik Elektromedik, Politeknik Kesehatan Kemenkes Surabaya Indonesia. This work is an open-access article and licensed under a Creative Commons Attribution-ShareAlike 4.0 International License (CC BY-SA 4.0).

2. MATERIALS AND METHODS

A. System Design

The detection system comprises four main components: a computer, a Data Acquisition System (DAQ), a multiplexer, and a multi-electrode sensor array. It employs the Analog Discovery 2, which integrates high-speed ADC and DAC for multi-frequency impedance detection. The setup uses two copper (Cu)-based electrodes, one with 64 points labeled U1–U64 and the other as ground. The use of a 64-electrode in Fig. 1. array was based on its ability to increase spatial resolution, as higher electrode density provides more detailed mapping of impedance distribution. This configuration allows for fine-grained reconstruction, especially in detecting localized anomalies, as supported by studies in electrical impedance tomography (EIT) where increased electrode count improves spatial accuracy [2]. The Analog Discovery 2 serves as the core DAQ device, handling signal generation, voltage measurement, and control via digital I/O. Although this study uses built-in DAQ tools, a more advanced calibration protocol (e.g., offset compensation and frequency response correction) was not implemented, and this is noted as a limitation that could be addressed in future iterations.

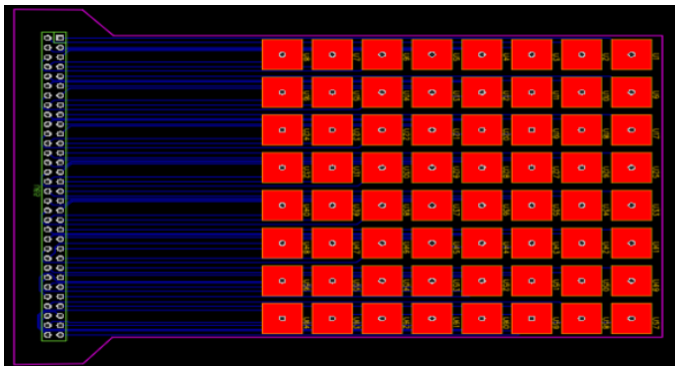

Fig. 1. Layout of the 64-Electrode Array Used

The selection of copper-based (Cu) electrodes is based on several advantages, such as mechanical stability, resistance to electromagnetic interference, and ease of mass fabrication with high precision [17]. This study integrates both hardware and software: the hardware includes a computer, Analog Discovery 2, multiplexer, 64-channel electrodes, reference resistor, and ground shown in Fig. 2. The computer, via the Waveform application, controls the multiplexer, frequency, and reference resistance, while the Analog Discovery 2 handles signal generation, oscilloscope functions, and digital I/O.

To improve signal fidelity, the system was tested in a low-interference environment. The entire setup was enclosed within a grounded metal frame to reduce electromagnetic interference. Shielded cables were used for all connections, and baseline noise measurements were taken prior to each recording to ensure consistent signal quality.

Furthermore, the WaveForms application will record impedance data from the 64-channel electrodes in Excel format. This dataset comprises the real, imaginary, and magnitude components of impedance for each electrode. Subsequently, a custom Delphi application processes this data and generates 8-bit RGB images by mapping the real, imaginary, and magnitude values to the red, green, and blue channels, respectively. Although this approach provides a basic image reconstruction method, more advanced algorithms such as the Gauss-Newton method or Total Variation regularization were not implemented. The RGB conversion approach, while intuitive, may limit the quantitative interpretation of internal conductivity changes and is best suited for qualitative analysis. More sophisticated reconstruction algorithms are recommended in future development [17], [18].

B. Experimental Setup

Our study utilizes both carrots and bengkoang as models

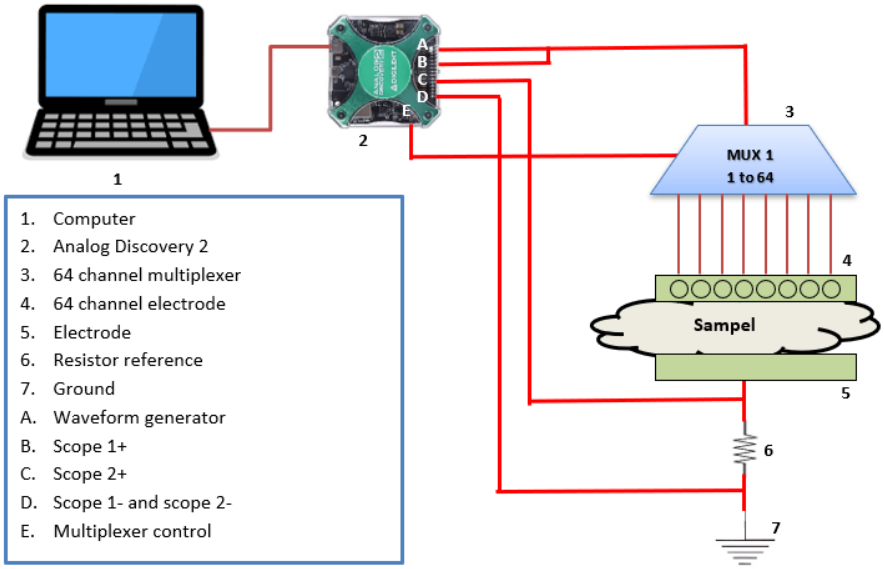

Fig. 2. The block diagram and workflow of the electrical impedance tomography for measurement

Corresponding author: Khushnul Ain, k_ain@fst.unair.ac.id, Biomedical Engineering Innovation Research Group, Faculty of Science and Technology, Universitas Airlangga, Surabaya, Indonesia
Digital Object Identifier (**DOI**): https://doi.org/10.35882/ijeeemi.v7i2.88
Copyright © 2025 by the authors. Published by Jurusan Teknik Elektromedik, Politeknik Kesehatan Kemenkes Surabaya Indonesia. This work is an open-access article and licensed under a Creative Commons Attribution-ShareAlike 4.0 International License (CC BY-SA 4.0).

for anomalies. All samples were carefully prepared by cutting them to a uniform thickness to ensure consistent measurements. Each sample was manually measured using a ruler, and the final thickness was confirmed to be 4 cm. This standardized sample preparation method is consistent with previous research in the field, such as the study by Zhang, Li, and Yang (2019), which highlighted the importance of uniform sample dimensions for reliable impedance measurements in EIT applications, and Tan et al. (2019), who reported similar preparation protocols to ensure measurement consistency [16], [19]. To ensure repeatability and minimize variability, five samples of each type (carrot and jicama) were prepared and measured. This allows for the estimation of variation and supports the statistical robustness of the results.

The anomaly will be placed at the center, arranged vertically between the 64-channel electrodes and the grounding electrodes. The electrodes are arranged facing each other or aligned in parallel, with the sample in the middle. To determine the optimal distance between the electrodes, an initial test was carried out with a variation of 4 cm, 5 cm, 6 cm, and 7 cm distances. This distance selection aims to evaluate its effect on the depth of penetration of electric current and the sensitivity of anomaly detection in the test medium. Similar approaches have been reported in recent studies, where variations in electrode spacing significantly influenced imaging quality and detection sensitivity in EIT systems [21].

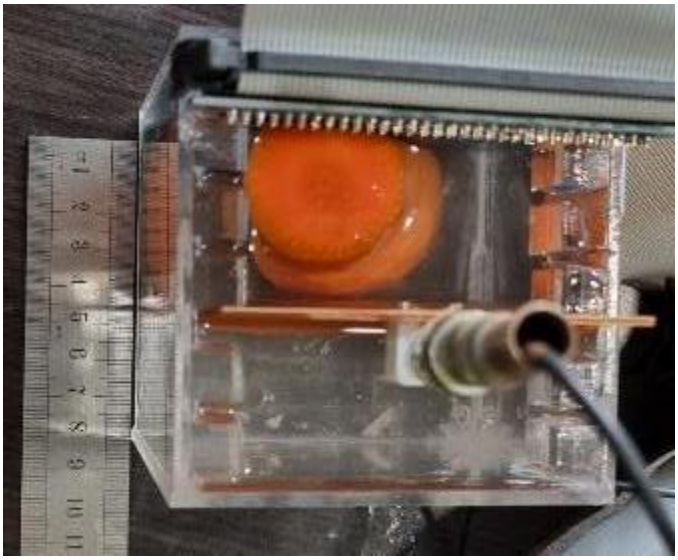

Fig. 3. The experimental setup that is used for the electrical impedance tomography measurement

The experiment was conducted in an air-conditioned room maintained at a temperature of approximately 24 – 25 °C to ensure environmental stability during data acquisition. An overview of the experimental setup is shown in Fig. 3. To improve measurement accuracy and reduce noise, each measurement point was repeated five times.

C. Signal Processing

When aiming to measure the impedance of biological samples in electrical impedance spectroscopy experiments, the electrical impedance, Z(ω), can be calculated using Eq. (5) as follows [21]:

$$\mathrm{Z}(\omega) = \frac{\mathrm{U}(\omega)}{I(\omega)} = R + jX(\omega) \tag{5}$$

where U is the voltage in the frequency domain, I is the current in the frequency domain, the real part of impedance is the resistance R, and the imaginary part is the reactance X(ω). The absolute value is calculated using Eq. (6) [21]:

$$|\mathrm{Z}| = \sqrt{(R)^2 + X(\omega))^2} \tag{6}$$

and the phase shift is calculated using Eq. (7) [21]:

$$\theta = arctan\ \frac{X(\omega)}{R} \tag{7}$$

In this study, impedance measurements were performed by injecting alternating current (AC) into the test object using the Analog Discovery 2 device. The injected current has a fixed frequency according to the selected (50 - 150kHz). Furthermore, the phase difference (θ) between the injection current and the measured voltage is analyzed to determine the impedance value (Z). Where R is resistance and Xc is capacitive reactance. The impedance value is calculated based on the relationship between resistance (R) and capacitive reactance (XC).

It can be calculated using Eq. (1) and Eq. (2) as follows [2]:

$$Z = \sqrt{R^2 + Xc^2} \tag{1}$$

$$\tan = \frac{Xc}{R} \tag{2}$$

where Z is the impedance, R is the resistance, XC is capacitive reactance, and θ is the phase difference. These equations can be used to determine the value of R and XC (Fig. 4). The values of R and XC are expressed by Equations Eq. (3) and Eq. (4) as follows [2]:

$$R = Zcos\theta \tag{3}$$

$$\mathrm{Xc} = Zsin\theta \tag{4}$$

The relation of R, Xc, and Z is shown in.

Corresponding author: Khushnul Ain, k_ain@fst.unair.ac.id, Biomedical Engineering Innovation Research Group, Faculty of Science and Technology, Universitas Airlangga, Surabaya, Indonesia
Digital Object Identifier (**DOI**): https://doi.org/10.35882/ijeeemi.v7i2.88
Copyright © 2025 by the authors. Published by Jurusan Teknik Elektromedik, Politeknik Kesehatan Kemenkes Surabaya Indonesia. This work is an open-access article and licensed under a Creative Commons Attribution-ShareAlike 4.0 International License (CC BY-SA 4.0).

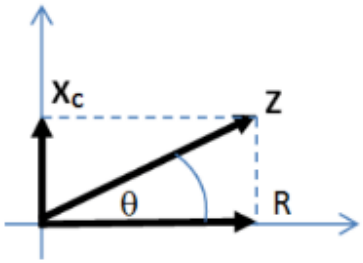

Fig. 4. The relation of Impedance, Capacitive Reactance, and Resistance measurement

D. Statistical Analysis

In this study, basic descriptive statistics were applied to evaluate the stability of impedance values obtained from five repeated measurements at each electrode point. Two key parameters were used: mean and standard deviation. The mean represents the average impedance value across repeated measurements Eq. (8). It serves as the central value summarizing the five repetitions conducted at each point.

$$Z^{-} = \frac{1}{n}\sum_{i=1}^{n} Zi \tag{8}$$

where Z^{-} is the average impedance, Z_i is the i-th impedance value, and n is the total number of repetitions. In this study, n=5 for each measurement point. Standard deviation quantifies the amount of variation or dispersion of the impedance values from the mean. A lower standard deviation Eq. (9) indicates that the repeated measurements are more consistent.

$$\sigma \sqrt{\frac{1}{n-1}\sum_{i=1}^{n}(Zi - Z^{-})^2} \tag{9}$$

where σ is the standard deviation, z_i represents each individual measurement, Z^{-} is the mean, and 'n' is the number of data points. The use of mean and standard deviation in this study aims to ensure that the data acquisition system produces reliable and repeatable impedance measurements.

3. RESULTS

A. Experimental Result

In this study, data were collected using a 64-electrode setup with electrode spacings of 4 cm, 5 cm, 6 cm, and 7 cm, all measured at a frequency of 50 kHz. The acquired data, including real impedance, imaginary impedance, and impedance magnitude, were initially stored in Excel format.

To evaluate the stability of the system, data collection was conducted five times under the same conditions. The impedance was measured across 64 electrodes in each experiment. The resulting graphs are shown in Fig. 5, Fig. 6, and Fig. 7. They show the distribution for all five trials. As observed, the impedance patterns across the electrodes are largely consistent, with similar trends and peak positions in each trial. Although there is a noticeable spike at some electrodes, the overall shape and values remain comparable. This indicates that the system demonstrates good stability, as repeated measurements yield similar impedance profiles.

Furthermore, each impedance component was individually plotted using Origin software to visualize the data. Subsequently, the data were imported into a Delphi-based application to generate 8-bit RGB images, where the impedance magnitude was mapped to the red channel (R), the real impedance to the green channel (G), and the imaginary impedance to the blue channel (B). This mapping facilitated the visualization of the electrical properties across the electrode grid. The system effectively visualized anomalies within the test medium, reflecting their positions. This approach aligns with findings from Sapuan et al. (2020), who demonstrated that separating real and imaginary impedance components enhances the detection of anomalies with similar overall

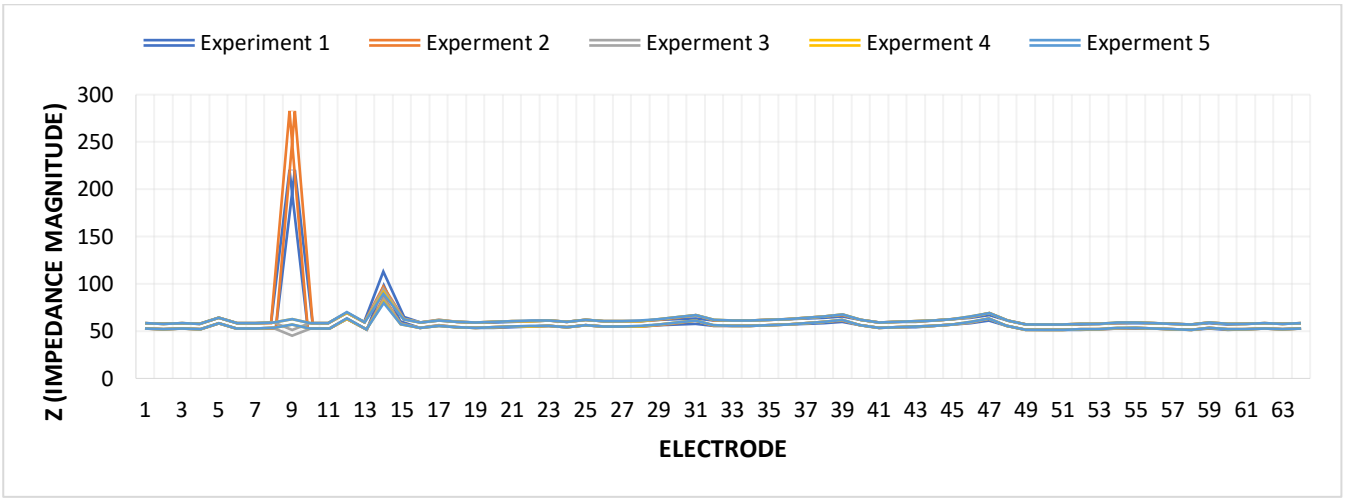

Fig. 5. Imaginary Impedance Variation Over Five Repetitions for System Stability Evaluation

Corresponding author: Khushnul Ain, k_ain@fst.unair.ac.id, Biomedical Engineering Innovation Research Group, Faculty of Science and Technology, Universitas Airlangga, Surabaya, Indonesia
Digital Object Identifier (**DOI**): https://doi.org/10.35882/ijeeemi.v7i2.88
Copyright © 2025 by the authors. Published by Jurusan Teknik Elektromedik, Politeknik Kesehatan Kemenkes Surabaya Indonesia. This work is an open-access article and licensed under a Creative Commons Attribution-ShareAlike 4.0 International License (CC BY-SA 4.0).

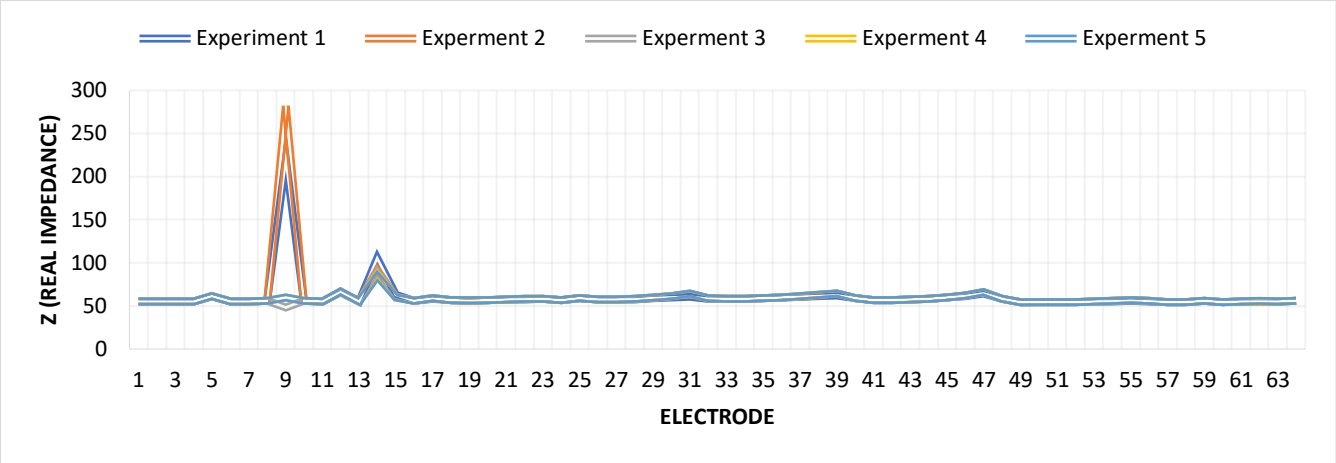

Fig. 6. Real Impedance Variation Over Five Repetitions for System Stability Evaluation

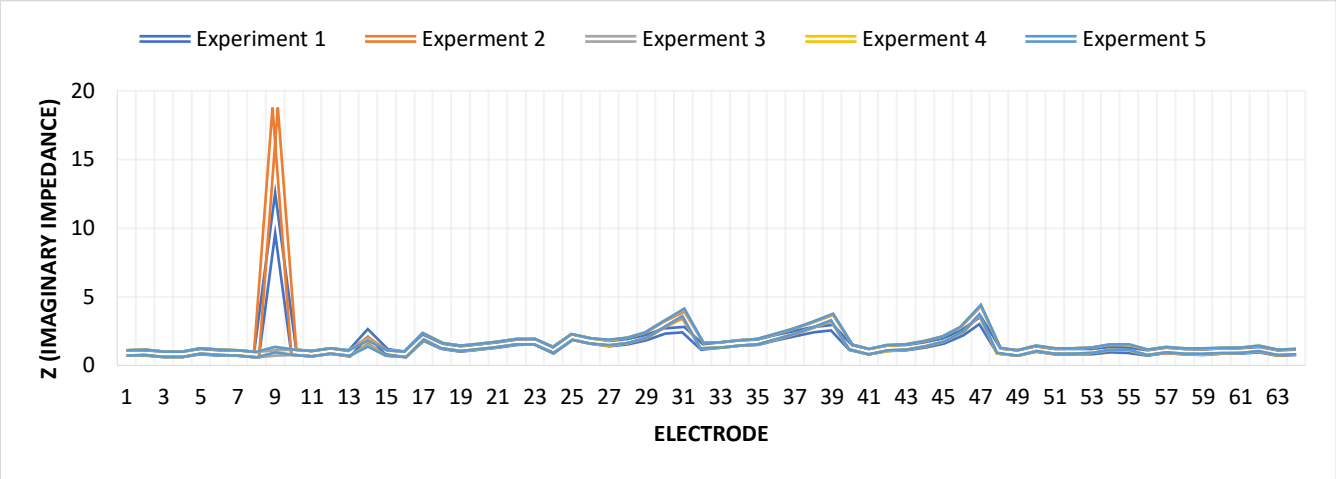

Fig. 7. Imaginary Impedance Variation Over Five Repetitions for System Stability Evaluation

impedance but differing resistive and capacitive properties [2]. Fig. 8 shows a comparison of the real impedance, imaginary impedance, and impedance magnitude diagrams of the carrot anomaly. The resulting RGB images reflect the positions of the anomalies within the test medium, corroborating recent studies that have shown advanced mapping techniques improve anomaly detection in EIT systems [22], [23], [24].

Based on our analysis, the electrode spacing of 4 cm provided the most accurate visualization, closely resembling the actual anomaly. This suggests that reducing the distance between electrodes enhances the system's ability to detect and represent anomalies effectively. Moreover, the analysis of the impedance components revealed that the imaginary impedance is particularly sensitive to changes in tissue properties, enabling superior anomaly detection compared to overall impedance measurements. This finding is consistent with previous research, which has demonstrated that the imaginary component of impedance responds more strongly to variations in tissue composition and permittivity, thereby improving anomaly detection capabilities [2], [26], [27].

Following the experiments conducted with the carrot anomaly, the next step involves performing similar tests using a jicama anomaly. These tests will be conducted at a frequency of 50 kHz, maintaining the same electrode distances as before: 4 cm, 5 cm, 6 cm, and 7 cm. The resulting RGB images reflect the positions of the anomalies within the test medium, corroborating recent studies that have shown advanced mapping techniques improve anomaly detection in EIT systems [23], [24], [25]. Same as the jicama anomaly, electrode spacing with 4cm has the best visualization. This suggests that reducing the distance between electrodes enhances the system's ability to detect and represent anomalies effectively. To investigate whether frequency affects anomaly detection, we varied the excitation frequency from 50, 80, 100, 120, and 150 kHz using a 4 cm distance. Recent research has shown that the frequency of the injected current in Electrical Impedance Tomography (EIT) significantly influences both the sensitivity and resolution of anomaly

Corresponding author: Khushnul Ain, k_ain@fst.unair.ac.id, Biomedical Engineering Innovation Research Group, Faculty of Science and Technology, Universitas Airlangga, Surabaya, Indonesia
Digital Object Identifier (**DOI**): https://doi.org/10.35882/ijeeemi.v7i2.88
Copyright © 2025 by the authors. Published by Jurusan Teknik Elektromedik, Politeknik Kesehatan Kemenkes Surabaya Indonesia. This work is an open-access article and licensed under a Creative Commons Attribution-ShareAlike 4.0 International License (CC BY-SA 4.0).

detection [17], [26]. Fig. 9 presents a visualization using 3D surface plots using Origin. Our experiments indicate that the images acquired at 50 kHz offer the most distinct representation of anomalies. The visualization at 50 kHz suggests that lower frequencies provide enhanced sensitivity for detecting conductivity differences, likely due to better current penetration and improved contrast between normal and anomalous regions. This finding is consistent with previous research showing that lower frequency ranges, such as 50 kHz, yield optimal imaging performance for anomaly detection in EIT applications [27], [28], [29].

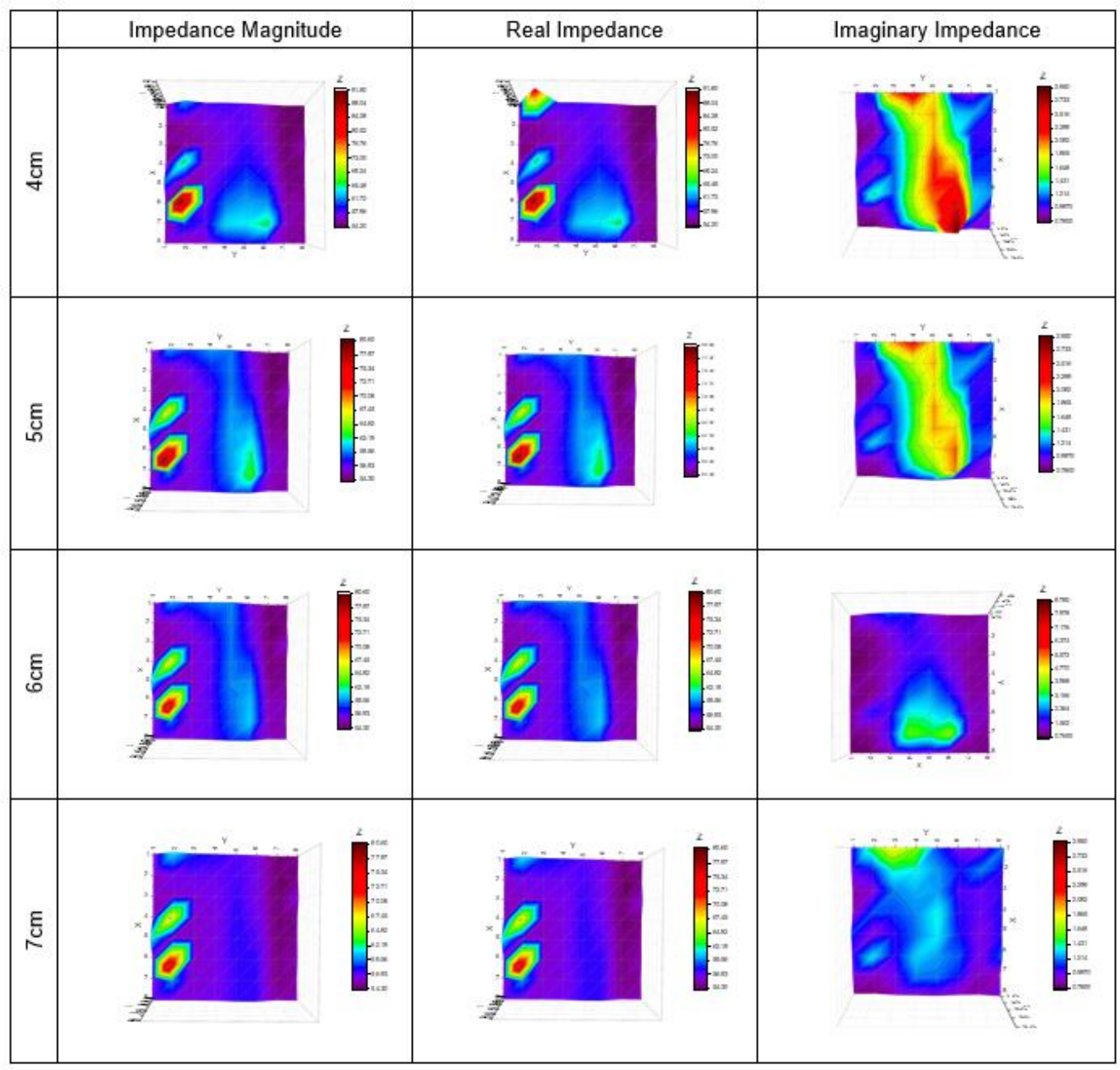

Fig 8. The comparison of the real impedance, imaginary impedance, and impedance magnitude diagrams of the carrot anomaly

Corresponding author: Khushnul Ain, k_ain@fst.unair.ac.id, Biomedical Engineering Innovation Research Group, Faculty of Science and Technology, Universitas Airlangga, Surabaya, Indonesia
Digital Object Identifier (**DOI**): https://doi.org/10.35882/ijeeemi.v7i2.88
Copyright © 2025 by the authors. Published by Jurusan Teknik Elektromedik, Politeknik Kesehatan Kemenkes Surabaya Indonesia. This work is an open-access article and licensed under a Creative Commons Attribution-ShareAlike 4.0 International License (CC BY-SA 4.0).

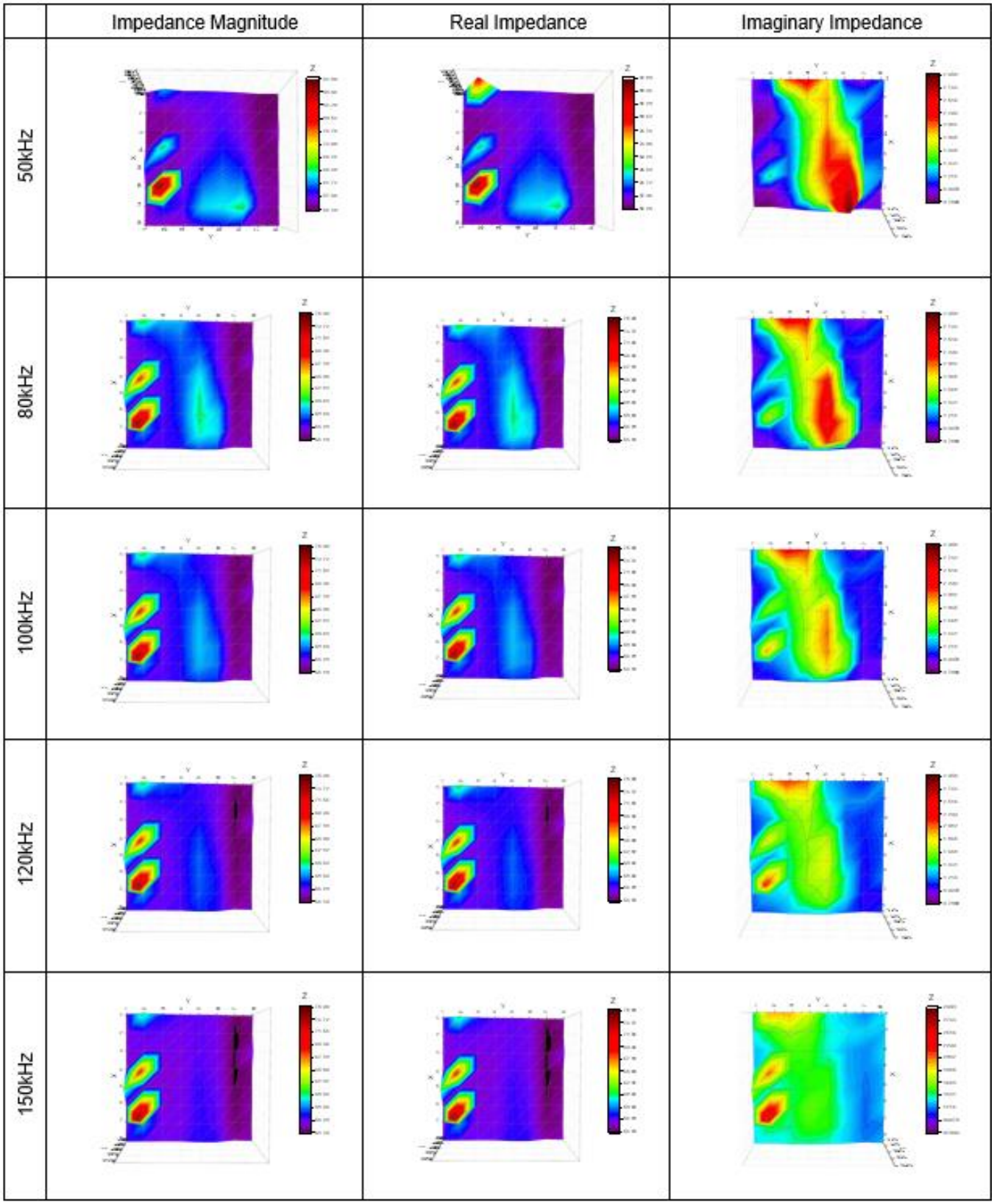

Fig 9. The comparison of the real impedance, imaginary impedance, and impedance magnitude diagrams of the carrot anomaly using frequency variance

Corresponding author: Khushnul Ain, k_ain@fst.unair.ac.id, Biomedical Engineering Innovation Research Group, Faculty of Science and Technology, Universitas Airlangga, Surabaya, Indonesia
Digital Object Identifier (**DOI**): https://doi.org/10.35882/ijeeemi.v7i2.88
Copyright © 2025 by the authors. Published by Jurusan Teknik Elektromedik, Politeknik Kesehatan Kemenkes Surabaya Indonesia. This work is an open-access article and licensed under a Creative Commons Attribution-ShareAlike 4.0 International License (CC BY-SA 4.0).

B. Analysis

Table 1 represents the average impedance values obtained during the experiment using frequency variance. Rs represents the real impedance value, and Xs denotes the imaginary impedance. Based on our analysis, we calculated the average impedance values at the tested frequencies and found that the highest average was obtained at 50 kHz. This quantitative result supports our visual observations, where the 3D surface plots generated at 50 kHz provided the clearest and most distinct representation of the anomalies.

In other words, the lower excitation frequency of 50 kHz appears to enhance the sensitivity and contrast in impedance measurements, thereby facilitating improved anomaly detection. This finding aligns with recent studies that have reported enhanced anomaly differentiation at lower frequencies in Electrical Impedance Tomography (EIT) [2], [27], [30].

Table 1. The Impedance Results with Frequency Variances Using Carrot and Jicama Anomaly

Anomaly	Freq (kHz)	Z Average (Ω)	Rs Average (Ω)	Xs Average (Ω)
Carrot	50	57.43	57.41	-1.27
	80	57.33	57.32	-1.34
	100	57.09	57.07	-1.35
	120	56.74	56.74	-1.35
	150	56.52	56.50	-1.44
Jicama	50	58.00	57.97	-1.78
	80	57.86	57.83	-1.83
	100	57.55	57.51	-1.84
	120	57.48	57.44	-1.93
	150	57.32	57.28	-1.06

This experiment measured the real impedance, imaginary impedance, and impedance magnitude and exported it as a CSV file. This CSV file is then uploaded into our custom Delphi application, which processes the data by calculating the average, maximum, and minimum values for each impedance component. Using this information, the application maps the data to generate an 8-bit RGB image, where the impedance magnitude is assigned to the red channel (R), the real impedance to the green channel (G), and the imaginary impedance to the blue channel (B).

The resulting RGB image effectively visualizes the spatial distribution of impedance across the electrode grid, enhancing anomaly detection. This approach to data mapping and visualization aligns with recent findings that emphasize the importance of multi-channel impedance data processing for improved image quality and sensitivity in EIT applications [31], [32]. The example of an 8-bit RGB image generated from the impedance data collected using a 4 cm electrode spacing at a frequency of 50 kHz, with a carrot anomaly, is shown in Fig. 10.

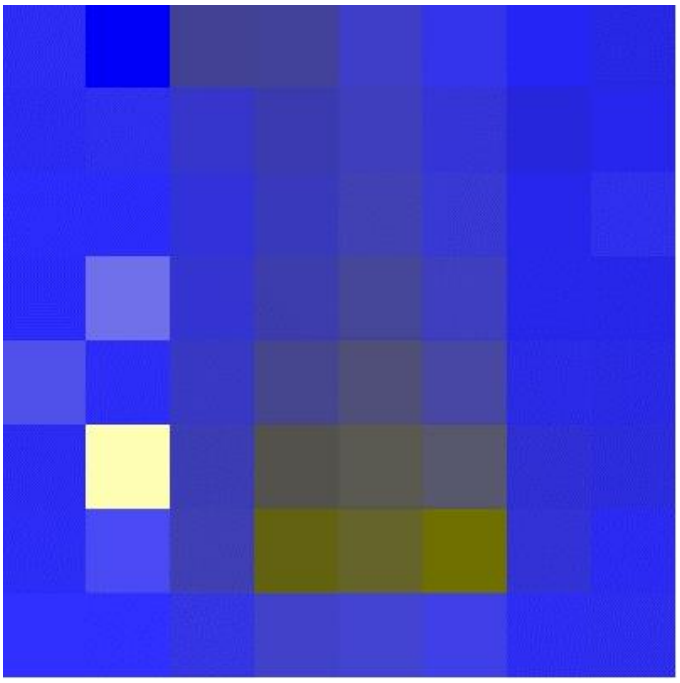

Fig. 10. The 8-bit RGB image at 4 cm distance and 150 kHz frequency using carrot anomaly

4. DISCUSSION

A paired sample t-test was performed to compare the impedance values obtained from the carrot and jicama anomalies. A significance value of < 0.05 indicates that there is a statistically significant difference between the two, confirming that these anomalies are indeed distinct. This study uses a NaCl 0.9% solution with a concentration of 100 mM as the measurement medium. The impedance of NaCl solution with a concentration of 100 mM at a frequency of 50–150 kHz ranges from 30–50 Ω. Meanwhile, the measurement results in this study showed that the carrot's impedance was around 56–59 Ω, and the jicama's was around 57–59 Ω. A comparison with the literature data showed that the results were still within a reasonable range [33].

The higher impedance observed in the biological samples compared to pure saline suggests that the intrinsic tissue structures (such as cell membranes, fiber content, and variations in intracellular electrolytes) act as additional barriers to electrical conduction, thereby increasing the overall impedance [34]. This behavior reflects the composite nature of biological tissues, where membranes behave like capacitors and intracellular fluids exhibit different conductivities compared to the extracellular environment.

In bioimpedance measurements, the applied frequency significantly influences the current's pathway through the tissue. At lower frequencies like 50 kHz, cell membranes behave like capacitors with high reactance, effectively preventing current from entering the cells. As a

Corresponding author: Khushnul Ain, k_ain@fst.unair.ac.id, Biomedical Engineering Innovation Research Group, Faculty of Science and Technology, Universitas Airlangga, Surabaya, Indonesia
Digital Object Identifier (**DOI**): https://doi.org/10.35882/ijeeemi.v7i2.88
Copyright © 2025 by the authors. Published by Jurusan Teknik Elektromedik, Politeknik Kesehatan Kemenkes Surabaya Indonesia. This work is an open-access article and licensed under a Creative Commons Attribution-ShareAlike 4.0 International License (CC BY-SA 4.0).

result, the current flows predominantly through the extracellular fluid, leading to a higher overall impedance. In contrast, at higher frequencies up to 150 kHz, the capacitive reactance of the cell membranes decreases, because capacitive reactance is inversely proportional to frequency, allowing the current to penetrate the intracellular space. This change typically results in a lower measured impedance, as the intracellular compartment usually offers less resistance than the extracellular environment. This frequency-dependent behavior helps differentiate between the extracellular and intracellular properties of biological tissues [32], [34], [35].

Repeated measurements showed consistent impedance patterns, suggesting high repeatability of the system. However, small fluctuations were still observed in certain electrodes. These variations may arise due to changes in contact impedance, slight movements of the anomaly, or environmental factors such as temperature and electrical noise. Despite these, the low standard deviation across repetitions reinforces the reliability and robustness of the measurement system.

The imaging results obtained through RGB mapping also reflects physiological implications. The real component (green channel) mainly represents resistive pathways and is influenced by ionic content, particularly in extracellular fluid. The imaginary component (blue channel), representing capacitive properties, is more sensitive to cellular membranes and tissue boundaries. These characteristics can help localize regions with structural differences, similar to the way physiological tissues are assessed in clinical EIT. Such component separation mimics physiological imaging used in diagnostics and enhances interpretation.

The frequency of 50 kHz showed the clearest contrast between anomalies and the surrounding saline. This supports findings from previous studies [27], [28], [29] that suggest low-frequency currents are more sensitive to extracellular impedance differences, making them more effective for surface-level anomaly detection. At higher frequencies (100–150 kHz), the impedance differences were less pronounced, possibly due to signal dispersion into intracellular compartments and reduced contrast.

Compared to Sapuan et al. (2020), who utilized only the imaginary impedance component to locate anomalies, our study extends this approach by combining both impedance components and mapping them onto RGB visualizations. Furthermore, our use of a denser electrode configuration (64 electrodes) allowed for higher spatial resolution and more accurate detection, which addresses the limitations observed in earlier studies that used fewer electrodes and did not consider multi-frequency effects [22], [23].

The system, equipped with 64 electrodes, enables the capture of detailed spatial impedance distributions, facilitating the identification of anomalies between saline, carrot, and jicama. This methodology is supported by previous studies, which have demonstrated that increasing the number of electrodes can significantly improve the sensitivity and accuracy of Electrical Impedance Tomography (EIT) systems [15], [16]. Additionally, the 4 cm spacing provided a balance between spatial resolution and signal stability, optimizing the quality of the reconstructed images.

Despite the promising results, this study has limitations. The use of static models and homogeneous saline background may not fully represent the complexity of biological tissues in clinical settings. Real human tissues exhibit layered structures, blood perfusion, and temperature variations, which could influence impedance measurements. Moreover, artifacts such as electrode polarization and edge effects were not explicitly modeled. Future research should focus on in vivo validation and include dynamic models to simulate physiological processes. Incorporating temperature control and calibration mechanisms could further improve system accuracy.

5. CONCLUSION

This study was conducted to develop an Electrical Impedance Tomography (EIT) system that can detect tissue anomalies by generating 8×8 RGB images from impedance data collected using 64 electrodes. The system was tested under different electrode spacings and excitation frequencies, and the best performance was observed when the electrodes were spaced 4 cm apart with a 50 kHz excitation frequency. Under these optimal conditions, the system produced the highest average impedance readings, 59.29 Ω for carrot and 57.96 Ω for jicama, indicating good sensitivity and accuracy in detecting anomalies. These results show that combining a dense electrode setup with RGB image mapping can effectively highlight differences in biological tissues based on their impedance characteristics. However, several limitations need to be addressed in future research. For example, the experiments were conducted at an estimated room temperature of 24–25°C without accurate temperature control, which might affect measurement consistency. Also, the electrodes were placed manually, which could lead to inconsistent contact and variation in data. To improve the accuracy and reliability of future measurements, it would be helpful to test with different types of solutions and a wider variety of biological samples. In the future, this method should be tested on more complex or realistic tissue models that better represent actual clinical conditions. Adding features like multi-frequency analysis and real-time image display could make the system more useful for practical applications. Finally, applying machine learning to automatically identify anomalies from the image data could make this technology even more effective and easier to use in medical diagnosis.

REFERENCES

[1] T. Huuhtanen and A. Jung, “Anomaly location detection with electrical impedance tomography using multilayer perceptrons,” in *IEEE International Workshop on Machine Learning for Signal*

Corresponding author: Khushnul Ain, k_ain@fst.unair.ac.id, Biomedical Engineering Innovation Research Group, Faculty of Science and Technology, Universitas Airlangga, Surabaya, Indonesia
Digital Object Identifier (**DOI**): https://doi.org/10.35882/ijeeemi.v7i2.88
Copyright © 2025 by the authors. Published by Jurusan Teknik Elektromedik, Politeknik Kesehatan Kemenkes Surabaya Indonesia. This work is an open-access article and licensed under a Creative Commons Attribution-ShareAlike 4.0 International License (CC BY-SA 4.0).

Processing, MLSP, IEEE Computer Society, Sep. 2020. doi: 10.1109/MLSP49062.2020.9231818.
[2] I. Sapuan, M. Yasin, K. Ain, and R. Apsari, "Anomaly detection using electric impedance tomography based on real and imaginary images," *Sensors*, vol. 20, no. 7, Apr. 2020, doi: 10.3390/s20071907.
[3] M. Zhao, H. Wi, E. J. Lee, E. J. Woo, and T. I. Oh, "Feasibility of anomaly detection and characterization using trans-admittance mammography with 60 x 60 electrode array," *Phys Med Biol*, vol. 59, no. 19, pp. 5831–5847, Oct. 2014, doi: 10.1088/0031-9155/59/19/5831.
[4] Mingkang Zhao, Hun Wi, Abu Hena Mostofa Kamal, Tong In Oh, I. Member, and S. M. I. and Eung Je Woo, *Feasibility study of a trans-admittance mammography (TAM) systemwith 36 00 current-sensing Electrodes*. IEEE, 2012.
[5] M. H. Choi, T. J. Kao, D. Isaacson, G. J. Saulnier, and J. C. Newell, "A reconstruction algorithm for breast cancer imaging with electrical impedance tomography in mammography geometry," *IEEE Trans Biomed Eng*, vol. 54, no. 4, pp. 700–710, Apr. 2007, doi: 10.1109/TBME.2006.890139.
[6] J. P. Leitzke and H. Zangl, "A review on electrical impedance tomography spectroscopy," 2020, *MDPI AG*. doi: 10.3390/s20185160.
[7] K. Ain, D. Kurniadi, Suprijanto, and O. Santoso, "Dual modality tran-admittance mammography and ultrasound reflection to improve accuracy of breast cancer detection," *J Teknol*, vol. 82, no. 4, pp. 117–124, Jul. 2020, doi: 10.11113/jt.v82.14491.
[8] S. Mansouri, Y. Alharbi, F. Haddad, S. Chabcoub, A. Alshrouf, and A. A. Abd-Elghany, "Electrical Impedance tomography – Recent applications and developments," 2021, *Universitetet i Oslo*. doi: 10.2478/joeb-2021-0007.
[9] M. Pessel and D. Gibert, "Multiscale electrical impedance tomography," *J Geophys Res Solid Earth*, vol. 108, no. B1, Jan. 2003, doi: 10.1029/2001JB000233.
[10] T. K. Bera, "Applications of Electrical Impedance Tomography (EIT): A Short Review," in *IOP Conference Series: Materials Science and Engineering*, Institute of Physics Publishing, Mar. 2018. doi: 10.1088/1757-899X/331/1/012004.
[11] S. Abasi, J. R. Aggas, G. G. Garayar-Leyva, B. K. Walther, and A. Guiseppi-Elie, "Bioelectrical Impedance Spectroscopy for Monitoring Mammalian Cells and Tissues under Different Frequency Domains: A Review," Dec. 21, 2022, *American Chemical Society*. doi: 10.1021/acsmeasuresciau.2c00033.
[12] M. Pasha, S. Kupis, S. Ahmad, and T. Khan, "A Krylov subspace type method for Electrical Impedance Tomography," *ESAIM: Mathematical Modelling and Numerical Analysis*, vol. 55, no. 6, pp. 2827–2847, Nov. 2021, doi: 10.1051/m2an/2021057.
[13] C. C. Chang *et al.*, "Electrical impedance tomography for non-invasive identification of fatty liver infiltrate in overweight individuals," *Sci Rep*, vol. 11, no. 1, Dec. 2021, doi: 10.1038/s41598-021-99132-z.
[14] A. Adler and A. Boyle, "Electrical impedance tomography: Tissue properties to image measures," *IEEE Trans Biomed Eng*, vol. 64, no. 11, pp. 2494–2504, Nov. 2017, doi: 10.1109/TBME.2017.2728323.
[15] H. Wi, H. Sohal, A. L. McEwan, E. J. Woo, and T. I. Oh, "Multi-frequency electrical impedance tomography system with automatic self-calibration for long-term monitoring," *IEEE Trans Biomed Circuits Syst*, vol. 8, no. 1, pp. 119–128, 2014, doi: 10.1109/TBCAS.2013.2256785.
[16] C. Tan, S. Liu, J. Jia, and F. Dong, "A wideband electrical impedance tomography system based on sensitive bioimpedance spectrum bandwidth," *IEEE Trans Instrum Meas*, vol. 69, no. 1, pp. 144–154, Jan. 2020, doi: 10.1109/TIM.2019.2895929.
[17] L. Yang *et al.*, "An Image Reconstruction Algorithm for Electrical Impedance Tomography Using Measurement Estimation of Virtual Electrodes," *IEEE Sens J*, vol. 22, no. 13, pp. 13012–13022, Jul. 2022, doi: 10.1109/JSEN.2021.3120190.
[18] C. Dimas, V. Alimisis, N. Uzunoglu, and P. P. Sotiriadis, "Advances in Electrical Impedance Tomography Inverse Problem Solution Methods: From Traditional Regularization to Deep Learning," *IEEE Access*, vol. 12, pp. 47797–47829, 2024, doi: 10.1109/ACCESS.2024.3382939.
[19] D. Minh Quan Cao *et al.*, "Development A Low-Cost Electrical Impedance Tomography System For Non-Invasively Detecting Abnormal In Breast Tissue-Phantom Study."
[20] J. Lee, K. Park, K. Park, Y. Kim, J. Kim, and S. Ryu, "Electrode Placement Optimization for Electrical Impedance Tomography Using Active Learning," *Adv Eng Mater*, vol. 26, no. 11, Jun. 2024, doi: 10.1002/adem.202301865.
[21] S. Nøvik *et al.*, "A CMOS Multi-Electrode Array for Four-Electrode Bioimpedance Measurements," *IEEE Trans Biomed Circuits Syst*, vol. 16, no. 6, pp. 1276–1286, Dec. 2022, doi: 10.1109/TBCAS.2022.3214243.
[22] A. Kojima, S. Yoshimoto, and A. Yamamoto, "Optimization of electrode positions for equalizing local spatial performance of a tomographic tactile sensor," *Front Robot AI*, vol. 10, 2023, doi: 10.3389/frobt.2023.1157911.
[23] R. Kumar and S. Tripathi, "A novel GUI-based image reconstruction algorithm of EIT imaging technique," *International Journal of Cognitive Informatics and Natural Intelligence*, vol. 15, no. 3, pp. 31–46, Jul. 2021, doi: 10.4018/IJCINI.20210701.oa3.
[24] Y. Wu, F. F. Hanzaee, D. Jiang, R. H. Bayford, and A. Demosthenous, "Electrical Impedance Tomography for Biomedical Applications: Circuits and Systems Review," *IEEE Open Journal of Circuits and Systems*, vol. 2, pp. 380–397, 2021, doi: 10.1109/OJCAS.2021.3075302.

Corresponding author: Khushnul Ain, k_ain@fst.unair.ac.id, Biomedical Engineering Innovation Research Group, Faculty of Science and Technology, Universitas Airlangga, Surabaya, Indonesia
Digital Object Identifier (**DOI**): https://doi.org/10.35882/ijeeemi.v7i2.88
Copyright © 2025 by the authors. Published by Jurusan Teknik Elektromedik, Politeknik Kesehatan Kemenkes Surabaya Indonesia. This work is an open-access article and licensed under a Creative Commons Attribution-ShareAlike 4.0 International License (CC BY-SA 4.0).

[25] H. Wang, E. Zimmermann, M. Weigand, H. Vereecken, and J. A. Huisman, "Comparison of different inversion strategies for electrical impedance tomography (EIT) measurements," *Geophys J Int*, vol. 235, no. 3, pp. 2888–2899, Dec. 2023, doi: 10.1093/gji/ggad398.
[26] M. Darbas, J. Heleine, R. Mendoza, and A. C. Velasco, "Sensitivity analysis of the complete electrode model for electrical impedance tomography," *AIMS Mathematics*, vol. 6, no. 7, pp. 7333–7366, 2021, doi: 10.3934/math.2021431.
[27] K. Ain, O. N. Rahma, A. P. Putra, N. Syavinas, D. Darmawan, and H. Sohal, "Bone fracture detection using electrical impedance tomography based on STEMlab Red Pitaya," *Indonesian Journal of Electrical Engineering and Computer Science*, vol. 32, no. 1, pp. 150–159, Oct. 2023, doi: 10.11591/ijeecs.v32.i1.pp150-159.
[28] J. Ma *et al.*, "Exploratory study of a multifrequency EIT-based method for detecting intracranial abnormalities," *Front Neurol*, vol. 14, 2023, doi: 10.3389/fneur.2023.1210991.
[29] G. Setyawan, P. A. Sejati, K. A. Ibrahim, and M. Takei, "Breast cancer recognition by electrical impedance tomography implemented with Gaussian relaxation-time distribution (EIT-GRTD)," *J Electr Bioimpedance*, vol. 15, no. 1, pp. 99–106, Jan. 2024, doi: 10.2478/joeb-2024-0011.
[30] M. Yasin, S. Böhm, P. O. Gaggero, and A. Adler, "Evaluation of EIT system performance," in *Physiological Measurement*, IOP Publishing Ltd, 2011, pp. 851–865. doi: 10.1088/0967-3334/32/7/S09.
[31] Q. X. Pan, Y. Li, N. Wang, P. F. Zhao, L. Huang, and Z. Y. Wang, "Variational Mode Decomposition-based Synchronous Multi-Frequency Electrical Impedance Tomography," *Information Technology and Control*, vol. 51, no. 3, pp. 446–466, Sep. 2022, doi: 10.5755/j01.itc.51.3.30014.
[32] B. Packham *et al.*, "Comparison of frequency difference reconstruction algorithms for the detection of acute stroke using EIT in a realistic head-shaped tank," *Physiol Meas*, vol. 33, no. 5, pp. 767–786, 2012, doi: 10.1088/0967-3334/33/5/767.
[33] E. Rahmawati, D. R. Santoso, J. A. F. Noor, and A. Nadhir, "Electrical impedance analysis of NaCl and CaCl2solutions based on equivalent electric circuit," in *Journal of Physics: Conference Series*, IOP Publishing Ltd, Jan. 2022. doi: 10.1088/1742-6596/2165/1/012025.
[34] C. Gabriel, S. Gabriel, and E. Corthout, "The dielectric properties of biological tissues: I. Literature survey," 1996. [Online]. Available: http://iopscience.iop.org/0031-9155/41/11/001
[35] R. J. Halter, A. Hartov, J. A. Heaney, K. D. Paulsen, and A. R. Schned, "Electrical impedance spectroscopy of the human prostate," *IEEE Trans Biomed Eng*, vol. 54, no. 7, pp. 1321–1327, Jul. 2007, doi: 10.1109/TBME.2007.897331.

AUTHOR BIOGRAPHY

Fransiska Maria Aprihapsari is currently pursuing her Master's degree in Biomedical Engineering at Universitas Airlangga, starting in 2024, with a specialization in medical instrumentation. She earned her Bachelor's degree in Applied Electromedical Technology Engineering from Politeknik Kesehatan Kemenkes Surabaya in 2023. Her research focuses on the development of medical instrumentation, particularly in designing and improving medical devices for clinical applications. Since 2021, Fransiska has been working as a practitioner in the field of medical equipment. She is keen to apply her practical knowledge to advance innovations that enhance the effectiveness of healthcare systems and patient care. She can be contacted at email: fransiska.maria.aprihapsari-2023@fst.unair.ac.id

Atin Asna Octavia is a postgraduate student in the Biomedical Engineering program at Universitas Airlangga, Surabaya, Indonesia, beginning her studies in 2024 with a focus on biomaterials. She earned her Bachelor's degree in Biomedical Engineering from the same university as part of the 2020 cohort and successfully graduated in 2024. Throughout her undergraduate journey, she was actively involved in student research and innovation programs. She received funding from the Ministry of Education, Culture, Research, and Technology (KEMDIKBUD) through the Student Creativity Program in Entrepreneurship (PKMK) in 2020 and the Student Creativity Program in Exact Research (PKMRE) in 2023. Her academic interests include biomaterials, tissue engineering, and biomedical product development. She can be contacted at email: atin.asna.octavia-2024@fst.unair.ac.id

Prof. Dr. Khusnul Ain, S.T., M.Si. is a professor of biomedical engineering at Universitas Airlangga, specializing in Electrical Impedance Tomography (EIT) and Electrical Impedance Spectroscopy (EIS). He earned his Bachelor's and Master's degrees from Universitas Gadjah Mada and a Doctorate from Institut Teknologi Bandung. His research focuses on improving EIT image reconstruction with machine learning, biomedical signal processing, and IoT-based healthcare systems. Committed to advancing medical diagnostics, he integrates physics, computing and engineering to develop non-invasive imaging

Corresponding author: Khushnul Ain, k_ain@fst.unair.ac.id, Biomedical Engineering Innovation Research Group, Faculty of Science and Technology, Universitas Airlangga, Surabaya, Indonesia
Digital Object Identifier (**DOI**): https://doi.org/10.35882/ijeeemi.v7i2.88
Copyright © 2025 by the authors. Published by Jurusan Teknik Elektromedik, Politeknik Kesehatan Kemenkes Surabaya Indonesia. This work is an open-access article and licensed under a Creative Commons Attribution-ShareAlike 4.0 International License (CC BY-SA 4.0).

technologies. Through interdisciplinary research, Prof. Khusnul Ain continues to enhance the accuracy and accessibility of biomedical engineering solutions for better healthcare outcomes. He can be contacted at email: k_ain@fst.unair.ac.id.

Bayu Ariwanto is a laboratory assistant at Universitas Airlangga, Surabaya, Indonesia, with a background in physics and biomedical engineering. He earned his Bachelor's degree in Physics from Universitas Airlangga in 2012, where his undergraduate research focused on the development of fiber optic sensors. He later completed his Master's degree in Biomedical Engineering from the same university in 2024. His current research interests include Electrical Impedance Tomography (EIT), Electrical Impedance Spectroscopy (EIS), bioimpedance, instrumentation, and medical device development. He is particularly interested in exploring non-invasive diagnostic technologies by combining engineering principles with biomedical applications. His work contributes to the advancement of medical instrumentation, aiming to improve the precision and practicality of diagnostic tools. He can be contacted at email: bayuariwanto@stafunair.ac.id

Corresponding author: Khushnul Ain, k_ain@fst.unair.ac.id, Biomedical Engineering Innovation Research Group, Faculty of Science and Technology, Universitas Airlangga, Surabaya, Indonesia
Digital Object Identifier (**DOI):** https://doi.org/10.35882/ijeeemi.v7i2.88
Copyright © 2025 by the authors. Published by Jurusan Teknik Elektromedik, Politeknik Kesehatan Kemenkes Surabaya Indonesia. This work is an open-access article and licensed under a Creative Commons Attribution-ShareAlike 4.0 International License (CC BY-SA 4.0).

Corresponding author: Khushnul Ain, k_ain@fst.unair.ac.id, Biomedical Engineering Innovation Research Group, Faculty of Science and Technology, Universitas Airlangga, Surabaya, Indonesia
Digital Object Identifier (**DOI):** https://doi.org/10.35882/ijeeemi.v7i2.88
Copyright © 2025 by the authors. Published by Jurusan Teknik Elektromedik, Politeknik Kesehatan Kemenkes Surabaya Indonesia. This work is an open-access article and licensed under a Creative Commons Attribution-ShareAlike 4.0 International License (CC BY-SA 4.0).